

pubs.acs.org/JPCA Article

Spectroscopic Manifestations of Indirect Vibrational State Mixing: Novel Anharmonic Effects on a Prereactive H Atom Transfer Surface

Published as part of The Journal of Physical Chemistry virtual special issue "125 Years of The Journal of Physical Chemistry".

Edwin L. Sibert III,* Karl N. Blodgett, and Timothy S. Zwier*



Cite This: J. Phys. Chem. A 2021, 125, 7318-7330



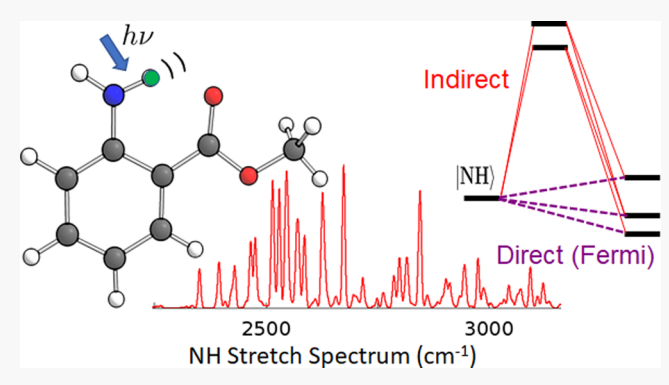
ACCESS

III Metrics & More

Article Recommendations

Supporting Information

ABSTRACT: The NH stretch region of the IR spectrum of methyl anthranilate is modeled in the S_1 state to understand the connection between the absence of this fundamental in the fluorescence-dip infrared spectra of Blodgett et al. [*Phys. Chem. Chem. Phys.* **2020**, 22, 14077] and its relevance to the H atom dislocation that occurs upon electronic excitation. A set of coordinates are chosen that highlight the role of certain low-frequency modes. A Hamiltonian is developed in which a large-amplitude two-dimensional surface describing the H-bonded H atom is linearly and quadratically coupled to the remaining degrees of freedom which are treated at the harmonic level. The surface is calculated within the time-dependent density functional theory framework by using the B3LYP/6-311++(d, p) level of theory with



dispersion. Our spectral results show that indirect couplings lead to massive intensity sharing over hundreds of wavenumbers. This sharing is predicted to be dramatically reduced upon deuteration. The spectral broadening mechanism is found to involve off-resonant doorway states that are themselves strongly coupled to states nearly degenerate with the NH stretch fundamental and represents a complementary mechanism to previous explanations based on Fermi resonance or the presence of Franck—Condon like combination bands with low-frequency motions. Consistent with the spectra predictions, time-dependent calculations show that if the NH stretch fundamental were excited with an ultrafast laser, it would decay within 40 fs. The competition between H atom dislocation and vibrational relaxation is discussed.

1. INTRODUCTION

As close analogues of salicylic acid and methyl salicylate, anthranilic acid (AA) and methyl anthranilate (MA) have been investigated as model compounds for excited state intramolecular proton transfer (ESIPT) reactions. These reactions occur in molecules where the hydrogen-bonding preferences change upon electronic excitation, leading to proton transfer (strictly speaking, H atom transfer) between donor and acceptor sites. Both experimental and theoretical studies showed that while there are substantial geometry changes upon electronic excitation in MA and AA, there is no evidence of complete hydrogen transfer in these molecules. Nevertheless, MA and AA undergo a less complete version of the full excited state reaction, sometimes termed H atom dislocation. Indeed, the recent work of Blodgett et al. demonstrated that in the NH(v=1) state the H-bonded H atom had an expectation value near the midpoint between the N and O atoms. Motivated by the possibility of seeing the shift from reactants toward H atom transfer products encoded in the infrared spectrum, these authors recorded excited state infrared spectra

from 1000 to 3600 cm $^{-1}$. The free NH stretch fundamental is readily observed at a frequency about halfway between the free NH $_2$ symmetric and antisymmetric stretch fundamentals; the H-bonded NH stretch transition is not recognizable in the spectrum. It is not often in spectroscopy that the most intense transition anticipated in the spectrum is not observable, and this provides a motivation for our work.

In systems where hydrogen bonding is present one often finds that, instead of the single transition that is expected upon excitation of an N-H or O-H bond, there are multiple transitions that are spread over a large frequency range. There are many theories for describing this so-called spectral broadening. One important source of broadening is due to

 Received:
 May 13, 2021

 Revised:
 July 22, 2021

 Published:
 August 12, 2021





multiple Fermi resonance interactions^{7–16} with modes that have approximately half the frequency of the high-frequency mode. Another source are the interactions that modulate the strength of the hydrogen bond, the broad line shape of the OH stretch in liquid water being the most famous example. Similar broadening has been observed in cold clusters and interpreted in an adiabatic framework. In such a picture, the effective potentials of low-frequency modes are altered upon vibrational OH or NH excitation, leading to Franck—Condon-like progressions in combination bands involving the hydride stretch and coupled low-frequency mode(s).

We have explored both possibilities in MA, and we were unable a find a representation that explains the spectral broadening based on these approaches. In this work we look for an alternative explanation for the missing NH stretch fundamental. We find that the above-mentioned Franck-Condon active modes act as doorway states. In the language used to describe vibrational energy relaxation, doorway states have the physical interpretation of arising from those zeroorder vibrations that are most strongly coupled via low-order anharmonic resonances to the initially localized zero-order bright state.8 In this work the local NH stretch state with one quantum of excitation is the bright state, and the doorway states are off-resonance, since they will always exceed the energy of the bright state by the frequency of the Franck-Condon-active mode. These doorway states are themselves coupled to states that are nearly degenerate with the bright state. Those coupling terms are due to higher order anharmonic terms that result from the rapidly changing forces along the normal modes as the H-bonded atom moves between the two possible H-bonding sites. We refer to this coupling through off-resonant doorway states as indirect coupling.

Following the ideas of Carrington and Miller²³ and others, ^{17,24} we incorporate these couplings into a two-dimensional surface Hamiltonian that is quadratically coupled to the remaining normal coordinates. We then solve the time-independent nuclear Schrödinger equation with a reduced dimensional model to predict the NH stretch contribution to the infrared spectrum of MA. Finally, we solve the time-dependent Schrödinger equation to examine the competing dynamics between motions associated with H atom dislocation and vibrational relaxation of the NH stretch back to the ground state.

The structure of this paper is as follows. In section 2 we review previous experimental and theoretical work on the S_0 and S_1 state surfaces of MA and AA. We highlight key vibrational modes needed to elucidate the fate of the NH stretch upon excitation in section 3. We also describe the construction of a force field that allows us to incorporate the influence of the modes in a Hamiltonian whose solution is discussed. Key results are presented in section 4, followed by a discussion in section 5.

2. BACKGROUND

In this section we review previous theoretical and experimental work on MA to clarify what is known to date about the S_1 excited state spectroscopy of this molecule. The molecule is shown in Figure 1, possessing an NH_2 group ortho to the methyl ester, so that one of its hydrogens is in an intramolecular H-bond with the C=O group of the ester. We have highlighted the relevant H atom by coloring it green in the figure. It is the vibrations associated with this proton that

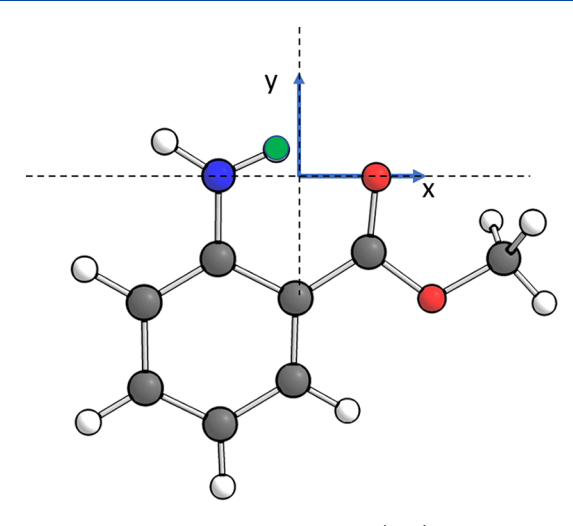


Figure 1. Structure of methyl anthranilate (MA). MA is the methyl ester of anthranilic acid (AA) having a methyl group in place of a H atom. The H atom undergoing dislocation is colored green. Oxygen and nitrogen atoms are colored red and blue, respectively.

are the focus of our paper. We now review the work that has sparked this interest.

Excitation to the S₁ state leads to an enhanced interaction between green the H atom and the nearby red oxygen atom. This enhancement is reflected in the electronic densities. Blodgett et al.³ calculated the electronic densities using TD-DFT methods for the S₀ and S₁ states and found a significant shift in electron density/negative charge from the NH₂ to the carbonyl group upon electronic excitation. This shift is similar to but less than that expected of a proton-coupled electron transfer and is reflected in the calculated geometry changes. The H-O hydrogen bond length is calculated to decrease from 1.93 to 1.72 Å upon excitation based on time-dependent density functional theory calculations²⁵ using the B3LYP hybrid functional in conjunction with Grimmes dispersion correction with Becke-Johnson damping²⁶ and the def2TZVP basis set. Similar results are obtained with the B3LYP/6-311+ +(d,p) level of theory by using Grimmes dispersion with the original D3 damping function.²⁷ Here the decrease is from 1.95 to 1.76 Å. All further calculations reported in this paper use the latter level of calculation. The above results are also consistent with the calculations of Sobolewski and Domcke, who found an analogous decrease in AA with the H-bond distances decreasing from 1.91 to 1.68 Å. They used the same level of theory with the cc-pVDZ basis set and no dispersion.

Consistent with this and other calculated geometry changes, the vibronic spectroscopy of jet-cooled methyl anthranilate (MA) and its water complex show long Franck—Condon progressions of in-plane modes, indicating significant heavy-atom rearrangement between the S_0 and S_1 electronic states. Accompanying these large geometry changes is extensive Duschinsky mixing involving both the in-plane and out-of-plane vibrations.

The geometric change between the two electronic states is less apparent in the pure vibrational spectra of the two states. Before discussing these differences, however, we briefly describe the fluorescence-dip infrared (FDIR) spectroscopy method 28 used to obtain these spectra. 4 In this scheme, a fixed UV probe laser (20 Hz) is tuned to be resonant with the $\rm S_0 - S_1$ origin transition, thereby promoting population to the zeropoint level in the $\rm S_1$ electronic state. The excitation laser is

temporally followed (10 ns) by a scanning IR laser. When the IR laser is resonant with a vibrational transition of the electronically excited molecule, absorption occurs, promoting the molecule to a vibrationally excited state in the S_1 manifold. The rate of nonradiative decay is increased relative to that of the initially excited level, resulting in a dip in fluorescence signal. The excited-state FDIR spectrum results from plotting the fluorescence depletion against the IR wavelength. In the absence of saturation effects and barring any mode-dependent nonradiative decay, the relative intensities of the lines are the same as those that would be predicted based on standard theories of infrared excitation of an initial state.

One of appealing features of the FDIR method is that it allows one to directly compare infrared spectra of ground and excited states. We have found for MA that there are several noteworthy differences. The S₁ spectrum shows a broadened C=O stretch transition at 1637 cm⁻¹ which is 83 cm⁻¹ lower in frequency than its ground state counterpart. The NH₂ bend shows a similar downward shift of 76 cm⁻¹ to 1557 cm⁻¹ in the excited state. The most pronounced differences, however, occur in the NH stretch regions. Figure 2 compares fluorescent-dip infrared spectra (FDIR) measured by Blodgett

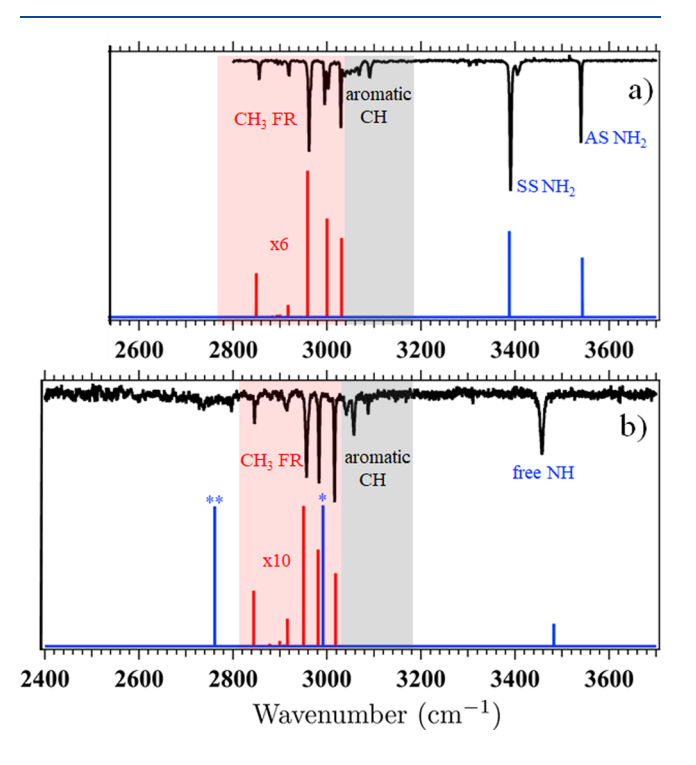


Figure 2. (a) Ground and (b) S₁ excited state FDIR spectra of MA from 2400 to 3700 cm⁻¹. The spectra are divided into four regions: NH stretch, aromatic CH stretch (shaded in gray), CH3 stretch (shaded in red), and low frequency. The experimental spectrum (black trace) is compared with the predictions of local mode modeling (stick spectra) in both electronic states. In both plots the red stick spectra corresponding to the CH3 Fermi mixed transitions are multiplied by the indicated scale factor for a more ready comparison with experiment. The dislocated NH stretch results are displayed as blue sticks in (b) with single and double asterisks indicating the corresponding calculated harmonic (2991 cm⁻¹) and anharmonic (2761 cm⁻¹) results. S₁ spectra were recorded down to 2400 cm⁻¹ to rule out the possibility of missing the NH stretch transition due to unexpectedly large anharmonic shifts of the fundamental. Reproduced with permission from ref 3. Copyright 2020 the PCCP Owner Societies.

et al.³ in the hybrid stretch region for the (a) ground and (b) excited electronic states. Three distinct sets of fundamental vibrational transitions appear. They are due to the NH₂, aromatic CH, and methyl CH stretches, the last of which is strongly perturbed with 2:1 Fermi resonance contributions with the CH scissor overtones. The anharmonic local mode model of those spectra,³ shown as stick diagrams below the experimental spectra, is in excellent agreement with the exception of the lower energy blue lines. We note that this model, which was developed to describe ground state vibrations, needed no special extensions to describe the excited state. This indicates that with the exception of the NH stretch the vibrations on both surfaces are well understood by using normal modes with standard anharmonicities and Fermi couplings.

The theoretical results shown in Figure 2b are consistent with expectations of H atom dislocation upon excitation. On the ground surface the NH₂ vibrations occur at 3390 and 3540 cm⁻¹, these corresponding to the symmetric and antisymmetric stretches, respectively. Upon excitation the non-H-bonded NH stretch transition (3457 cm⁻¹) is shifted to near the center of the two ground state vibrations, and the H-bonded NH stretch drops to 2991 cm⁻¹ or even lower when anharmonicity is explicitly included. The frequency lowering, which is due to the hydrogen bonding, is accompanied by an enhanced intensity of the lower frequency transition. In fact, we have had to increase the CH stretch intensities by a factor of 10 in the lower plot so that they can be clearly seen alongside the much more intense NH fundamental. Surprisingly, the H-bonded NH stretch transition does not appear in the experimental results of the lower plot. This situation is not unique to MA. Sobolewski and Domcke⁵ have calculated IR spectra for AA for the ground and S₁ states in Figure 2 of their paper. Their spectra are similar to the theoretical results of Figure 2 with the obvious exception of the pink shaded regions of the latter. Experimentally, Southern et al. observed a small peak near the expected position. The intensity of this transition, even when anharmonic effects are included,6 is dramatically overestimated by theoretical calculations.

Blodgett et al.³ explored the reason for the missing NH stretch fundamental. Carrying out an adiabatic separation that treats the dislocated NH stretch as the high-frequency mode, they found that when this mode is excited and all the remaining modes are allowed to relax, the geometry changes are sufficiently great that the H atom becomes equally shared between the blue N and red O atoms of Figure 1. They conjectured that these geometry changes, accompanied by the energy lowering of the adiabatic NH $\nu=1$ state, would lead to Franck–Condon factors and spectral dilution. In this work we strive to incorporate the couplings responsible for these geometry changes into a solution of the nuclear Schrödinger equation to ascertain whether these couplings can lead to a disappearance of the NH stretch due to fast relaxation processes.

There are two key mechanisms that lead to spectral broadening in molecules that are vibrationally excited at low temperatures. ²⁹ The first is due to vibrational Franck—Condon factors. The excitation of an OH stretch is known to lead to enhanced hydrogen bonding. This in turn can lead to structural rearrangement. Although this arrangement is typically associated with the rearrangement of a solvent in hydrogen-bonded systems, ²⁹ these effects extend to cold molecular clusters for both OH and NH stretch excita-

tion. $^{17-22}$ The second broadening mechanism is vibrational coupling via cubic Fermi resonances or higher order resonances to nearby states. In hydrogen-bonding environments both NH and OH stretch excitation can lead to fast relaxation via these couplings. $^{9,11-14,30}$

Constructing simple Hamiltonians that included the couplings responsible for Franck—Condon broadening and relaxation via Fermi couplings, we find that neither leads to extensive broadening of the NH fundamental. Moreover, if there were strong Fermi couplings, one would expect that their presence would have been revealed in the anharmonic calculations of Egidi et al. To determine which mechanism, if any, is at play, we turn to an examination of the potential surface and a search of coordinates that would reveal the relevant couplings.

3. THEORETICAL METHODS

In this section we motivate a model for describing what we believe are the most relevant motions leading to rapid relaxation of the H-bonded NH stretch. These motions are incorporated into a potential energy surface and a model Hamiltonian. The solution of this Hamiltonian is then described.

3.1. Coordinates and Potential. To guide the discussion we return to Figure 1, which shows the structure for MA. The dislocated H atom (green) is described by coordinates x and y where the x-axis lies along the N-O atom axis with the origin of the coordinate system halfway between these two atoms. The three coordinates of interest are x, y, and 2d, the distance between the N (blue) and O (red) atoms. With the exception of the H-bonded H atom, the remaining internal coordinates are the standard Z-matrix coordinates based on stretches, bends, and dihedral angles. The relevant subset of these coordinates will be introduced after a discussion of the potential.

Borgis and Hynes³¹ developed an insightful model for describing proton tunneling

$$A-H\cdots A' \leftrightarrow A\cdots H-A'$$

in liquids based on two degrees of freedom: Q, the distance between A and A', and q, the distance from the A—A' bond center. More closely related to the MA molecule is malonaldehyde, which undergoes proton tunneling between equivalent sites within the same molecule. In that case, the A and A' correspond to oxygen atoms, whereas in MA A = N and A' = O. Giese et al. ¹⁷ in their review article provide a nice example of the importance of this mode, calculating the presence of Franck—Condon progressions in the O—O vibration upon OH stretch excitation. Extending the above ideas to our system, the distance 2d can be identified as the Q coordinate that modifies the barrier associated with the H atom transfer described by q. Figure 3 shows the V(x,y) potential with d constrained to a value close to the equilibrium position.

The surface is obtained using the Gaussian program²⁵ by carrying out partial optimizations in which the positions of the H-bonded H atom and the nearby O and N atoms are held fixed in space, with the O and N atoms constrained to lie on the x-axis equidistant from the origin. We performed 14×10 calculations on an $\{x, y\}$ grid of the H atom's coordinates. Throughout this paper the molecule is constrained to have C_s symmetry, which it does for the S_1 potential minimum at the level of theory used in this work.

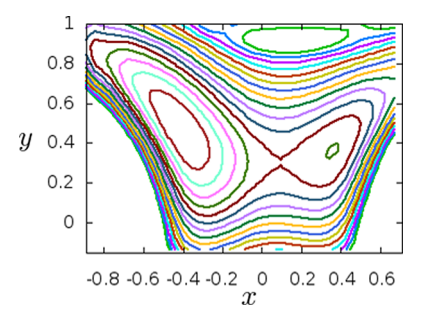


Figure 3. Equipotential energy contours as functions of the $\{x, y\}$ distances defined in Figure 1. All other coordinates are relaxed except for d, which is fixed at 1.33 Å. Contours are spaced at 1000 cm⁻¹ intervals.

The contours shown in the figure, drawn at 1000 cm⁻¹ intervals, are the result of a two-dimensional cubic spline fit. The contours clearly show a small second minimum at $\{x, y\} \approx \{0.4 \text{ Å}, 0.4 \text{ Å}\}$ that is consistent with the formation of an O–H bond. However, on the basis of the figure, one would not expect this second minimum to significantly affect the shape of the NH stretch fundamental wave function, since the energy of this configuration is greater that of a state with a single quantum of excitation in an NH stretch.

Figure 4 shows the $\{x, y\}$ potential energy landscape as a function of d. This figure highlights the central role of the N-

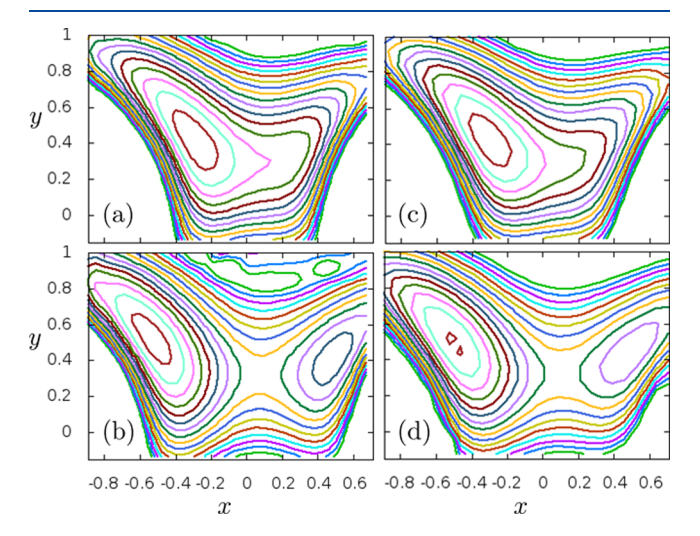


Figure 4. Equipotential energy contours as functions of the $\{x, y\}$ distances defined in Figure 1. All coordinates are relaxed except for d, which is fixed at (a) 1.25 Å and (b) 1.41 Å. Contours are spaced at 1000 cm^{-1} intervals. In (b) the unexpected wiggles in the energy contours at high energies and large y values are associated with the presence of a second excited electronic state. (c) and (d) are the same as (a) and (b), respectively, except that contours are results for the quadratic potential of eq 1.

O bond distance. Panels a and b of Figure 4 have d = 1.25 Å and d = 1.41 Å, respectively. The potential contours show that these changes in d are associated with small amounts of energy yet allow for larger low-energy extensions of the H atom along the x-coordinate.

So far we have identified interesting potential features that indicate that H atom motion might strongly couple to other modes on the S_1 electronic surface. We now consider the form of the Hamiltonian and the choice of coordinates that allow us to solve the nuclear Schrödinger equation for this system.

Perhaps the best approach would be to model the surface by treating d as one of the internal coordinates and then develop a reaction surface that has the remaining modes coupled to this three-dimensional $\{x, y, d\}$ surface. Instead, we have chosen a more approximate and less expensive approach based on the equilibrium structure and the fact that analytic Hessians are now available for excited state calculations. 25 We expand the potential in terms of the internal coordinates to second order

$$V = V_0 - \mathbf{f}^T \mathbf{S} + \frac{1}{2} \mathbf{S}^T \mathbf{F} \mathbf{S}$$
 (1)

where $\{V_0, \mathbf{f}, \mathbf{F}\}$ are the potential, forces, and force constant matrix written as functions of x and y when all the remaining internal coordinates are held at their equilibrium values. The coordinates S are bond and angle extension coordinates. We also calculate the dipole and its derivatives as

$$\mathbf{d} = \mathbf{d}_0 + \mathbf{D}^T \mathbf{S} \tag{2}$$

where $\{\mathbf{d}_0, \mathbf{D}\}\$ are the dipole components and their derivatives calculated in an Eckart frame. The results for $\mathbf{d}_0(x,y)$ are shown in Figure 5. The reorientation of the dipole vectors illustrates the charge transfer that is associated with the large amplitude H atom motion.

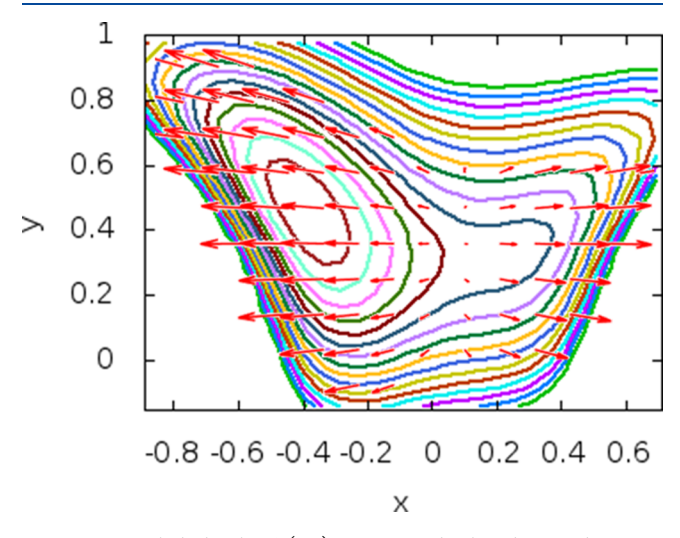


Figure 5. Scaled dipole $\mathbf{d}_0(x,y)$ moment displayed as red arrows overlaying potential contours of $V_0(x,y)$ of eq 1. Contours are spaced at 1000 cm⁻¹ intervals from 1000 to 18000 cm⁻¹. Dipoles are calculated in an Eckart frame that corresponds to the frame shown in Figure 1 in the equilibrium position.

The model parameters are calculated by using the Gaussian suite. For each $\{x, y\}$ point we extract the energy, Cartesian forces, Hessian, dipole, and its derivative and convert to internal coordinates. The grid of points is substantially more dense than those used to explore the potential features in Figures 3 and 4, as our calculations use basis sets based on discrete variable representations (DVR).³² The grid includes 30 equally spaced points in the x direction running from -1.009 to 0.818 Å and 18 points in the *y*-direction running from -0.2 to 1.5 Å.

To test whether the potential expansion retains the interesting features associated with dislocation presented above, we regenerate the potential contours of Figure 4 using the potential of eq 1 by minimizing this potential subject to the constraint that d takes on a specific value. As mentioned previously, in all calculations the molecule is constrained to have C symmetry. While this is true for the minimum, there are several out-of-plane modes where displacements along xand y lead to imaginary frequencies. We expect that inclusion of these modes will lead to spectral congestion but not contribute to the short time dynamics due to the weaker couplings and low frequencies of these modes. We also freeze the internal bending coordinates of the phenyl ring. These constraints are also needed to ensure that all the eigenfunctions of F remain positive over the full range of the grid. The results of the minimization, shown in Figures 4c and 4d, are similar to those obtained from those of Figures 4a and 4b, respectively. The approximate potential qualitatively reproduces the central role of the d coordinate and the relaxation of the other modes as functions of the $\{x, y\}$

pubs.acs.org/JPCA

Because of the computational cost of high-dimensional solutions to the Schrödinger equation, we consider a reduced dimensional, 11-DOF Hamiltonian that includes nine of the internal coordinates plus the x and y DOF. The choice of coordinates, described in the Supporting Information, is based on the values of the forces f given in eq 1. The coordinate d is a function of six of the coordinates that are included.

In Figure 6a,b we compare IR spectra based on the harmonic oscillator/linear dipole approximation. The results in (a) are obtained from diagonalizing the internal coordinate F and G matrices. They are essentially equivalent to the frequency results of an equilibrium Gaussian calculation²⁵ and, as a result, provide a check of our coordinate

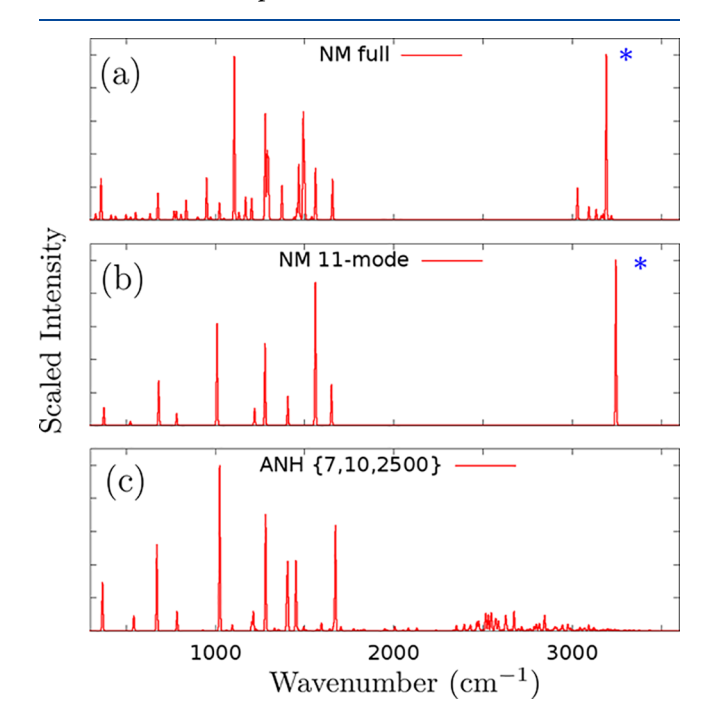


Figure 6. Normal mode linear dipole IR spectra (a) for all 54 vibrational degrees of freedom of MA and (b) for the 11-DOF reduced dimensional normal mode Hamiltonian described in the text. The intense transition near 3200 cm⁻¹, marked with an asterisk, is due to the dislocated NH stretch excitation. (c) Spectrum of the anharmonic 11-DOF model Hamiltonian of section 3.2. The basis set for this calculation is defined by three quantities $\{M, N, I\}$, discussed below in the text. All results are for the S₁ electronic surface.

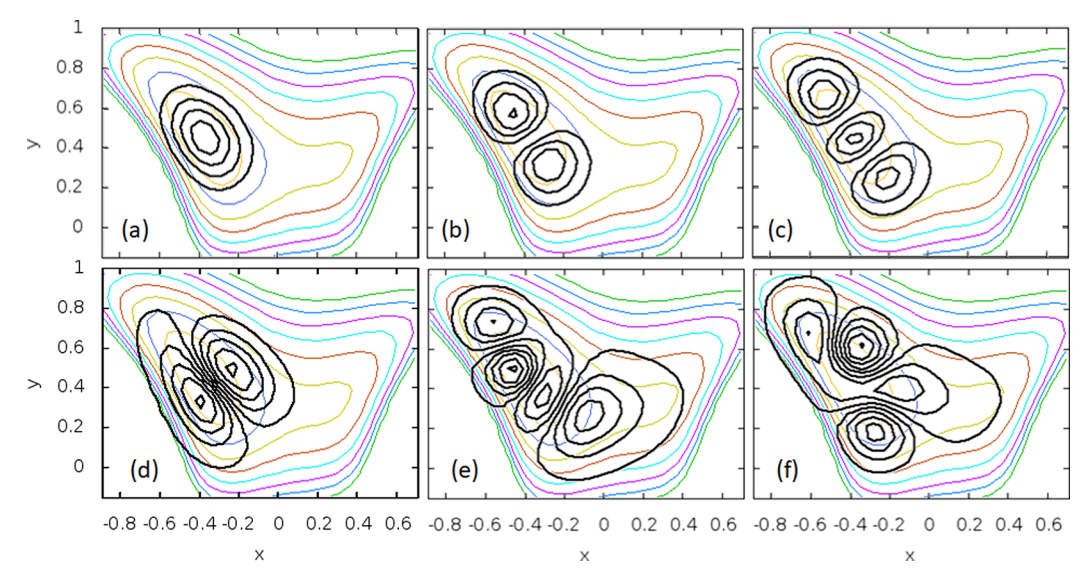


Figure 7. Six lowest energy wave functions (black) corresponding to n = 1-6 of eq 5 describing the x and y degrees of freedom with the remaining coordinates constrained to the equilibrium values. The corresponding transition energies out of n = 1 (a) are 1301.6, 2592.3, 2775.1, 3822.9, and 3959.2 cm⁻¹. Potential energy contours are shown at 2000 cm⁻¹ intervals. The fourth state (d) is nominally the state with one quantum of NH stretch.

transformations. The results in (b) are obtained by setting to zero all the **F** and **G** matrix elements that are not included in the 11-DOF Hamiltonian. These matrices are provided in the Supporting Information. In (a) the nonbonded NH stretch at $3645~\rm cm^{-1}$ is outside the axis range. The H-bonded NH stretch at $3191~\rm and~3244^{-1}$ in the full and $11-\rm DOF$ model are reasonable results for hydrogen-bonded NH stretches.

In a previous study,³ we were able to assign all the prominent features at the high-frequency end of the IR spectra with the exception of H-bonded NH stretch. Using the above-described model, we now consider solutions to the nuclear Schrödinger equation that shed light on the absence of the NH stretch transition theoretically predicted to be an intense transition in both Figure 2b and Figure 6a,b.

3.2. Anharmonic Hamiltonian and Basis Sets. The coordinate choice presented in the previous section leads to a simple approximate form for the kinetic energy contribution to the Hamiltonian

$$\hat{T} = \frac{1}{2} [G_{xx} p_x^2 + G_{yy} p_y^2] + \frac{1}{2} \sum_{i=1}^9 \sum_{j=1}^9 P_i G_{ij} P_j$$
(3)

where P_i is the momentum conjugate to S_i . We treat the kinetic contribution at the harmonic level and ignore the coordinate dependencies of the Wilson G-matrix elements.³³ These elements are not functions of x or y. In addition to the harmonic approximation, we neglect the kinetic coupling of the $\{x, y\}$ DOF to the other vibrational coordinates. This coupling is small due to the light proton and the choice of the $\{x, y\}$ internal coordinates. We assume that $G_{xx} = G_{yy} = 1.0297$ amu⁻¹, the equilibrium value for G_{xx} . In fact, the diagonal elements lie in the range 1.026-1.051 amu⁻¹, and the coupling G_{xy} element varies between -0.014 and 0.026 amu⁻¹. These weak dependencies and small couplings are also a result of the coordinate choice and the light mass of the proton.

To solve the corresponding Schrödinger equation, we use a product basis that is obtained following a two-step process. We first solve for the $\{x, y\}$ DOF assuming the internal coordinates take on the values of the equilibrium configuration (S = 0).

The ground state eigenfunction is then used to average over the $\{x, y\}$ -dependent forces and force constants of eq 1 to obtain a potential used to solve for the remaining internal coordinates. These steps are now described in more detail.

Using a sinc DVR³² based on the 30 \times 18 grid of $\{x, y\}$ points described above, we find the eigenvalues $E_n^{(x,y)}$ and eigenfunctions of the pure H atom Hamiltonian contribution to the combined potential (eq 1) and kinetic (eq 3) contributions of the full Hamiltonian. The Hamiltonian is

$$\hat{H}^{x,y} = \frac{1}{2} G_{xx} [p_x^2 + p_y^2] + V_0 \tag{4}$$

Only those 399 points for which V_0 is less than 19000 cm⁻¹ are included in the 2D-DVR calculation. The resulting eigenkets are expressed as a linear combination of the DVR kets $|\chi_k\rangle$ centered on the points $\{x_k, y_k\}$ as

$$|\Psi_n\rangle = \sum_k |\chi_k\rangle \langle \chi_k |\Psi_n\rangle \tag{5}$$

We tested the results with respect to the grid spacing, increasing the number of grid points from $\{N_x, N_y\} = \{30, 18\}$ to $\{36, 24\}$, and none of the 15 lowest eigenstates changed by more than 1 cm⁻¹. The six lowest energy wave functions and the corresponding transition energies, obtained from this latter calculation, are shown in Figure 7. Panels b and c show states with one and two quanta of CNH bend excitation, respectively; panel d shows a state with one quantum of NH stretch excitation.

The final Hamiltonian is set up as a direct product of N of the lowest energy kets described above and a harmonic oscillator basis $|\mathbf{v}\rangle$ describing the \mathbf{S} degrees of freedom. The product form of the potential of eq 1 leads to easy evaluation of the matrix elements. Carrying out the integration over the $\{x, y\}$ DOF leads to

$$\langle \Psi_n | \hat{H} | \Psi_m \rangle = E_n^{(x,y)} \delta_{n,m} + \left[\frac{1}{2} \sum_{i=1}^9 \sum_{j=1}^9 P_i G_{ij} P_j \right] \delta_{n,m} - \left[\mathbf{f}^T \right]_{n,m} \mathbf{S}$$

$$+\frac{1}{2}\mathbf{S}^{T}[\mathbf{F}]_{n,m}\mathbf{S} \tag{6}$$

The force constant and force matrix elements are easily evaluated in the DVR. For example, we evaluate the force matrix elements as

$$[\mathbf{f}]_{n,m} \equiv \langle \Psi_n | \mathbf{f} | \Psi_m \rangle = \sum_k \langle \Psi_n | \chi_k \rangle \mathbf{f}(x_k, y_k) \langle \chi_k | \Psi_m \rangle \tag{7}$$

where we have used the DVR property that

$$\langle \chi_k | f(x, y) | \chi_k' \rangle = f(x_k, y_k) \delta_{k,k}, \tag{8}$$

Evaluating the full Hamiltonian matrix only requires linear and quadratic simple harmonic oscillator matrix elements of the position and momentum operators. The convergence of the resulting variational calculation is improved if we convert to normal modes $S = LQ_i$ where the choice of the normal modes is based on the force constant matrix $[F]_{n,n}$ where n corresponds to the ground state. The size of the harmonic oscillator basis $|\mathbf{v}\rangle$ is controlled by a single parameter M_i ; only those basis functions for which $\sum_i \nu_i$ is less than M are included in the basis.

In the remainder of this paper we use f and F to represent the linear and quadratic terms of the Hamiltonian of eq 6 regardless of whether we use internal or normal coordinates. From a computational perspective, the form of the Hamiltonian remains the same, but the numerical values of these matrix elements change depending on the choice of normal or internal coordinates. This feature has the advantage that we can check the computer code used to set up the Hamiltonian matrix by ensuring that the variational results are independent of the n value that is chosen in defining the normal modes and independent of whether we use internal or normal coordinates. To make these comparisons, we reduced the number of internal coordinates to three, so that the energy spacing and intensities could be converged regardless of the choice of internal or normal coordinates.

The Hamiltonian in the $|\Psi_n\rangle|\mathbf{v}\rangle$ basis has many zero elements. This spareness is ideal for iterative methods for solving the Schrödinger equation. To obtain spectra, we follow the three stage approach of Stanton. We first use the Davidson method to calculate $|\Phi_{\rm gs}\rangle$, the ground state eigenfunction of the full Hamiltonian, as a linear combination of the basis $|\Psi_n\rangle|\mathbf{v}\rangle$. We then evaluate $d_x|\Phi_{\rm gs}\rangle$ and $d_y|\Phi_{\rm gs}\rangle$, where d_x and d_y are in in-plane components of the dipole given by eq 2. We provide details of these calculations in the Supporting Information. These vectors are the starting vectors for the Lanczos method, 36 which, as an output, provides the eigenvalues E_k and the eigenfunction expansion coefficients $A_{a,k} = \langle \Phi_k | d_a | \Phi_{\rm gs} \rangle$. The spectral intensities are calculated as

$$I_k = (A_{x,k}^2 + A_{x,k}^2)E_k (9)$$

We investigate the short-time dynm via a numerical solution of the time-dependent Schrödinger equation

$$\Psi(x, y, \mathbf{Q}, t) = \sum_{n} \sum_{\mathbf{v}} c_{n, \mathbf{v}}(t) |\Psi_{n}\rangle |\mathbf{v}\rangle$$
(10)

using the method of Askar and Cakmak³⁷ in which the coefficients evolved as

$$\mathbf{c}(t + \Delta t) = \mathbf{c}(t - \Delta t) - 2i\Delta t \mathbf{H} \mathbf{c}(t)$$
(11)

In practice, c is a time-dependent vector whose index is based on a mapping of the n and the v quantum numbers. For clarity, however, we retain the double subscripts in our discussion. This solution method complements the Lanczos method as both require matrix multiplication of the Hamiltonian matrix and a vector. As we are looking at short times, more sophisticated methods were not needed. Convergence of the results is checked with respect to the choice of basis sets, described above, and the size of the time step Δt used in the numerical integration. Using time steps of 0.033 and 0.0167 fs yields probability results that are indistinguishable in plotted form.

Our motivation for this approach stems from the fact that in our model Hamiltonian basis $|\Psi_n\rangle|v\rangle$ the only basis state that carries oscillator strength in infrared absorption of the ground vibrational state on the S_1 surface is the $|\Psi_4\rangle|0\rangle$ state whose $\{x,y\}$ dependence is shown in Figure 7. This state corresponds to excitation of the NH stretch, and following the literature, we refer to this state as a bright state. Nesbitt and Field⁸ in their review article beautifully describe how dynamics occurs as a result of this state being made up of a linear combination of eigenstates

$$|\Psi_{\text{bright}}\rangle \equiv |\Psi_4\rangle|\mathbf{0}\rangle = \sum_i c_i |\Phi_i\rangle$$
 (12)

Embedded in the subsequent dynamics of this state is encoded the infrared spectrum. More specifically, following Heller, ³⁸ the Fourier transform of the overlap of the bright state with itself $\langle \Psi_{\text{bright}}(t)|\Psi_{\text{bright}}(t=0)\rangle$ is proportional to the high-frequency portion of the spectrum. In addition to providing an alternative way to calculate a spectrum, the time-dependent study allows us to follow probability flow once it leaves the initial bright state. This information is not directly encoded in the IR spectrum. We also note that Blodgett et al. ⁴ report that the S_1 state is well isolated from other excited electronic states, so that multistate vibronic coupling can be discounted as a contributing factor for the missing band.

Using the time-dependent approach, we calculate the magnitude squared of the above quantity as well as two additional quantities. In our calculation the magnitude squared is the time-dependent probability of being in an initially prepared state $P_{\rm NH}(t) = |c_{4,0}|^2$. The corresponding basis state $|\Psi_4\rangle|0\rangle$, shown in Figure 7d, corresponds to one quantum of NH stretch excitation and no quanta of excitation in the remaining modes. Second, following ideas based on density matrices, we integrate over the **Q** degrees of freedom to obtain

$$P(x, y) = \int d\mathbf{Q} |\Psi(x, y, \mathbf{Q}, t)|^{2}$$

$$= \sum_{n} \sum_{m} \sum_{\mathbf{v}} c_{m,\mathbf{v}}^{*} c_{n,\mathbf{v}} \Psi_{m}^{*}(x, y) \Psi_{n}(x, y)$$

$$\equiv \sum_{n} \sum_{m} d_{m,n} \Psi_{m}^{*}(x, y) \Psi_{n}(x, y)$$
(13)

where the diagonal elements $P_n = d_{n,n}$ are the probabilities of being in a given state $|\Psi_n\rangle$ of the $\{x, y\}$ DOF system. Borrowing an analogy from the description of vibronic states, if the $|\Psi_n\rangle$ corresponded to electronic states rather than vibrational states, then $d_{4,4}$ would correspond to the probability of being in the third excited electronic state and $|c_{4,0}|^2$ would correspond to the probability of being in the third electronic

state and having no quanta of vibrational excitation. The third quantity we evaluate is the time-dependent probability, P(x,y), for the $\{x, y\}$ DOF.

4. RESULTS

The results are shown in Figure 6c for a calculation with $\{M, N, I\} = \{7, 10, 2500\}$, where M is the number of $|\Psi_n\rangle$ basis functions and the N determines the size of the harmonic oscillator basis set $|v\rangle$. Specifically, a function is included if $\sum_i v_i < N$. The third variable I is the number of Lanczos iterations. One can see that the low-energy region of the spectrum is essentially unaffected, whereas the NH stretch region is dramatically altered. The NH stretch transition, shown as a single line, in panels a and b fractures when the anharmonic effects are included. Figure 8 shows this region in more detail

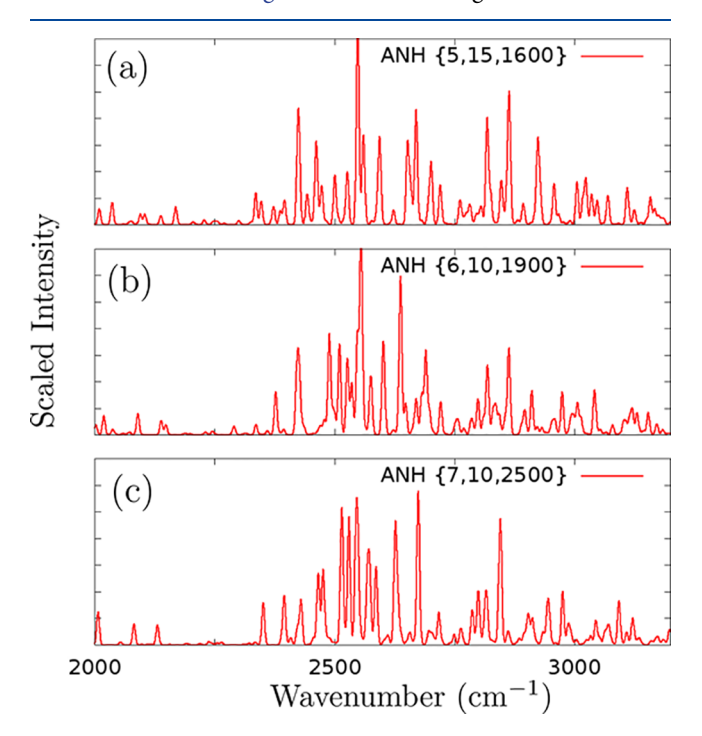


Figure 8. Anharmonic results of the 11-DOF model Hamiltonian at three different levels of calculation at higher resolution than the results of Figure 6. The calculations are defined by three quantities $\{M, N, I\}$ discussed in the text. Individual transitions are modeled as Gaussian line shapes with FWHM = 7 cm⁻¹.

for three different basis sets as denoted by the $\{M, N, I\}$ values. Although the details vary, the overall picture of intensity sharing over hundreds of wavenumbers is consistently reproduced. We believe that these results suggest that this level of intensity sharing spread over almost $1000~\rm cm^{-1}$ dilutes the oscillator strength to the point that the NH stretch fundamental is not identifiable in the experimental IR spectrum.

A possible way to test this conjecture would be to compare theory to experiment for a deuterated MA molecule in which one replaces the H-bonded hydrogen with a deuterium. When we repeat the calculation with the increased mass G_{xx} in eq 4, we obtain the results of Figure 9. Our model predicts significantly less mixing upon deuteration than that shown in Figure 6. Most of the intensity resides in one or two lines depending on the level of theory used in the vibrational

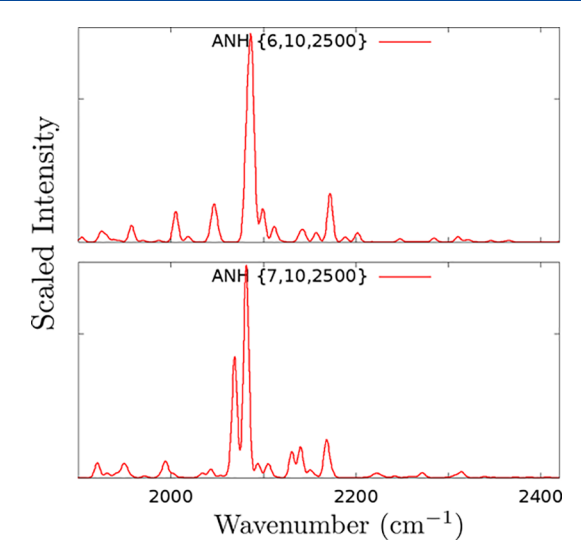


Figure 9. Spectra of the deuterated H-bonded ND stretch for two different levels of theory for the 11-DOF model Hamiltonian on the S_1 surface. Individual transitions modeled as Gaussian line shapes with FWHM = 7 cm⁻¹.

calculation. Unfortunately, no experiments on such a deuterated sample have yet been performed to our knowledge.

It is also interesting to compare the S_1 results to those of the electronic ground state. The FDIR spectra of MA, shown in Figure 2, display a pair of symmetric and antisymmetric NH stretches at 3380 and 3540 cm $^{-1}$, respectively, that are well understood. To a good approximation, the only states to which the two NH stretches are coupled are to themselves. Because our 11-DOF model neglects the NH stretch that is not involved in the hydrogen bonding, it should predict a single high-frequency transition corresponding to excitation of the NH stretch that is hydrogen bonded on the S_1 surface.

Figure 10 compares ground state results for the (a) normal mode 11-DOF Hamiltonian to (b) those obtained from the corresponding 11-DOF anharmonic Hamiltonian. The similarity of these two results contrasts sharply with the analogous S₁ comparison of Figure 6b,c results. On the S₁ surface the anharmonic couplings lead to extensive mixing, and on the S₀ surface the biggest differences are some minor anharmonic shifts that arise from the anharmonicity of the NH stretching and bending degrees of freedom. Because the same coordinates and basis sets are being used in both of the anharmonic calculations, the differences between the two surfaces are due to the significant enhancement of vibrational couplings on the S₁ surface. We also note that the nonbonded NH stretch is not present in either of the two 11-DOF models. The choice of modes to include was designed for treating the NH vibrations on the S₁ surface, where these vibrations are well separated in

The width of the spectral features in Figure 8 is consistent with fast (<0.1 ps) probability flow out of the NH stretch upon ultrafast excitation. The spectra, however, do not tell us where the probability flows. To answer this question, we adopt a time-dependent perspective. Figure 11 shows probability flow assuming an initial state $|\Psi_4(x,y)\rangle|0\rangle$, a basis state shown in Figure 7d that closely resembles one quantum of excitation of the NH stretch with no excitation in the normal modes. We tested the convergence of these results by using basis sets defined by two quantities $\{M, N\}$, discussed previously; we

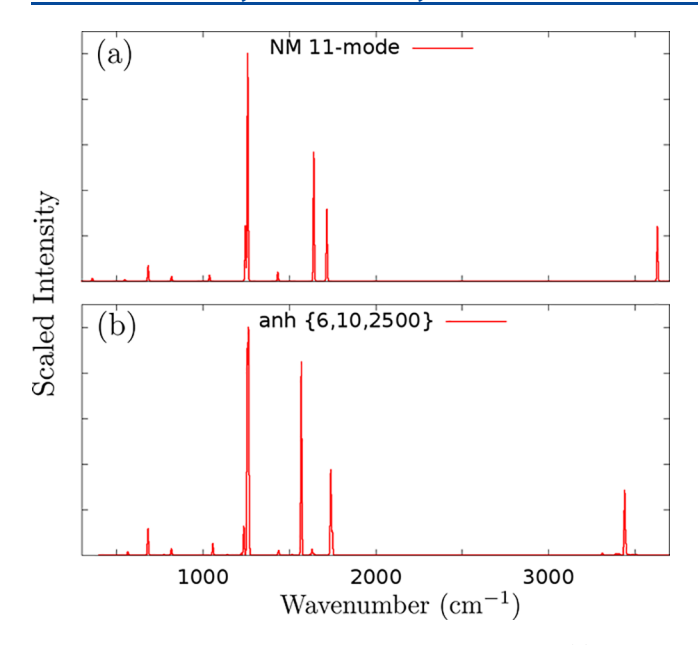


Figure 10. S_0 spectra of the H-bonded NH stretch for (a) the 11-DOF normal mode Hamiltonian and (b) the anharmonic 11-DOF model Hamiltonian. Individual transitions modeled as Gaussian line shapes with FWHM = 7 cm⁻¹.

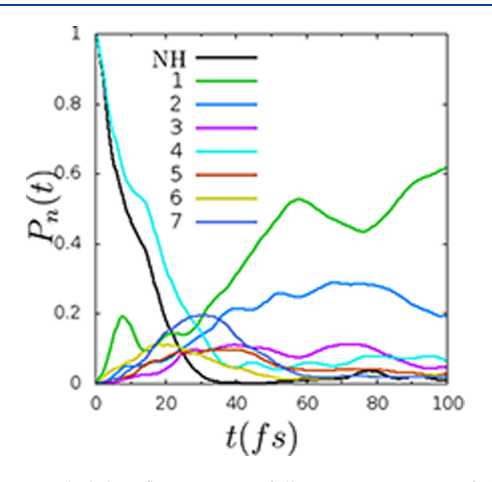


Figure 11. Probability flow vs time following excitation of the zero-order NH stretch states, six of which are shown in Figure 7. $P_{\rm NH}$ (black) is the probability of being in the initial state. Remaining probabilities are the diagonal elements of the density matrix $P_n = d_{n,n}$ (n = 1-7) (see eq 13).

find that $\{5, 12\}$ results shown in the figure and $\{6, 15\}$ results (see Figure S2) show only minor differences at longer times.

Figure 11 shows that the probability of being in this state, $P_{\rm NH}$, goes nearly to zero within 40 fs. The remaining plots show the diagonal elements, P_n , of the density matrix of eq 13. Specifically, the cyan line, associated with P_4 , corresponds to the probability of having one quantum of NH stretch excitation. As mentioned above, the difference between P_{NH} and P_4 is due to the latter including contributions from states with one quantum of excitation in the NH and some additional excitation in the normal modes. The large values of P_1 and P_2 that grow in after about 50 fs indicate that by this time most of the probability is in the ground and first excited state of the $\{x, x\}$ y} DOF. We also observe at short times (15–50 fs) that there is substantial excitation in n > 4 states. Looking at the corresponding functions in Figure 7, we see that these states have amplitude along the low-energy path associated with H atom dislocation.

To access the dynamics associated with the H-bonded H atom in more detail, we plot the solution to the time-dependent Schrödinger equation assuming the same initial state as above. The solution is plotted in the form of a probability distribution function P(x, y), defined in eq 13, which is obtained by averaging the full probability over the Q DOF. The result is shown in Figure 12. One observes the H-bonded H atom initially (20-40 fs) moves toward the bonding site of the O atom as the probability is rapidly decaying out of the excited NH stretch. Consistent with the probability flow results of Figure 11, after about 50 fs most of the probability has returned to the ground and first excited state. The excess bend excitation is evident in the greater extent of the probability along the bend coordinate at latter times compared to that of the initial state.

5. DISCUSSION

Although the description of the coupling mechanisms that lead to the absence of the NH stretch varies depending on the representation, there are several insights that our work provides. The first insight is that of the potential features highlighted in Figures 3 and 4. These potentials clearly show significant stretch bend coupling and a low pathway to hydrogen atom dislocation. One expects that these features might impact a spectrum, and, indeed, this is what we have demonstrated.

It is interesting to consider the mechanisms that lead to the fractionated spectra of Figure 8. The form of the Hamiltonian

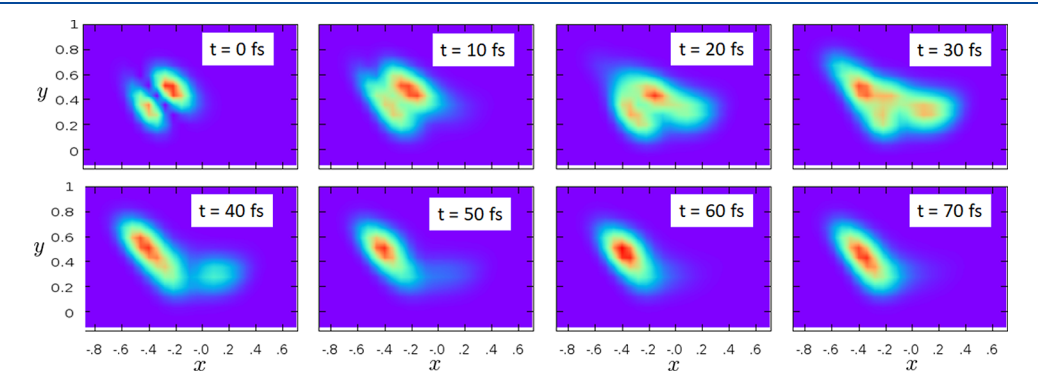


Figure 12. Time evolution of the initial prepared probability P(x,y) (see eq 13) for a state initially corresponding to one quantum of excitation in the NH stretch. The full wave function is averaged over **Q** DOF.

has close similarities to those used in modeling vibronic spectra where the $\{x, y\}$ DOF correspond to the electronic DOF and where the internal coordinates are expanded about the same values for all surfaces. The changes in $[F]_{n,n}$ from one n value to the next lead to Duschinsky rotations. These rotations are due to changes in the harmonic force fields of two different electronic states. In our work the $[\mathbf{F}]_{n,n}$ are the harmonic force fields for the n high-frequency states of Figure 7. One also has geometry changes upon electronic excitation that result in Franck-Condon factors. In our work we include the shifts in the harmonic potentials that occur upon excitation by adding linear terms to the expansion. The larger the linear term, the larger the geometry shifts and the greater the Franck-Condon factors; the nine $[f]_{4,4}$ values describe the size of the nine linear terms in the potential expansion. We provide the matrices for the ground state and the basis state that most closely resembles the NH stretch excited state in the Supporting Information.

Our separation of the fast $\{x, y\}$ and slow S degrees of freedom is diabatic rather than adiabatic, so one must not press the analogy too far. Nevertheless, Franck—Condon factors cannot be the primary reason for the spectral congestion, since these would lead to intensity sharing at higher energies than what we observe. The lowest frequency in the anharmonic model is around 400 cm^{-1} , and any progression in that mode would have that spacing.

In our model, the congestion is due to a complicated set of indirect couplings, and large basis sets are needed to obtain reasonably converged results. Nevertheless, one can turn off and on various coupling pathways to highlight which of these pathways are important. We introduce a concrete example to clarify the discussion. Figure 13 illustrates one of the pathways

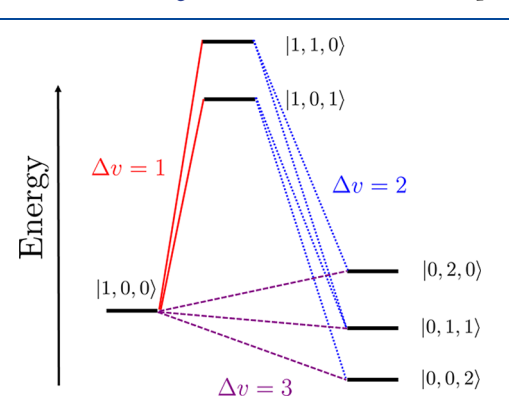


Figure 13. Schematic energy level diagram showing coupling pathways between states $|n_1, n_2, n_3\rangle$ of a three-dimensional system. Here mode one is roughly twice the frequency of the other two modes. The mixing pathways are distinguished by the total change in vibrational quanta $\Delta \nu$ of the coupled states. The $\Delta \nu = 3$ Fermi coupling is indicated by the purple dashed line. The $\Delta \nu = 1$ coupling, denoted by the red lines, can lead to Franck—Condon-like transitions. The blue dashed lines represent $\Delta \nu = 2$ couplings that in a normal mode representation would be due to quartic couplings such as $Q_1^{\ 3}Q_2$. See the text for details.

that contributes to the strong mixings. We present it to illustrate the importance of indirect couplings and to connect the couplings present in our model with more traditional normal mode approaches.

This simplified schematic includes select members of a direct product basis $|n_1, n_2, n_3\rangle$. The n_1 quantum number describes the quanta of NH stretch excitation. More precisely

 $n_1 = 0$ and 1 correspond to the n = 1 and n = 4 states of the $|\Psi_n\rangle$ basis states shown in Figure 7. The remaining two quantum numbers correspond to excitation in the normal mode basis of two select modes with frequencies 1139 and 1619 cm⁻¹. We chose these two since the combination band of the two is one that is nearly degenerate with the NH stretch.

As the tier model of Figure 13 shows, these states could be directly coupled by Fermi couplings. These are shown as $\Delta \nu =$ 3 couplings, since the NH fundamental is coupling to an overtone or combination states of the lower frequency modes. In a simple model of stretch-bend Fermi coupling, the potential contribution to the Fermi matrix element arises from the bend force constant being a function of the bond length, this dependence leading to a potential term of the form $f_{sbb}sbb$ where s and b are the stretch and bend coordinates, respectively. These couplings are included in our model since the force constants are functions of x and y in eq 1. In the present example, the Fermi coupling term is included in the $[F]_{14}$ proportional contribution of eq 6. As mentioned above, the n = 1 and n = 4 refer to the states of eq 5 with no excitation and one quantum of NH stretch excitation, respectively. We find, however, that even when we set $[F]_{nm} = 0$ for all $m \neq n$, there is still significant fractionation of the NH fundamental. Because of the weak couplings, these Fermi coupled states do not serve as doorway states.

We now consider a second pathway for state mixing that involves coupling through doorway states that are off-resonant with the initial states. These doorway states correspond to a $\Delta \nu$ = 1 transition. These couplings are a result of the excitation of the NH stretch leading to a change in bond length or angle of one or more of the internal coordinates. In an adiabatic representation, these couplings would lead to Franck-Condon factors. If the frequency of the two low-frequency normal modes were to decrease, the Fermi coupling would decrease, since the states that are initially in resonance would detune. In contrast, the $\Delta v = 1$ coupling at play here becomes more pronounced since the energy separation between the coupled states is proportional to the frequency of the normal modes. Importantly, these doorway states are themselves coupled to states nearly degenerate with the initial state. This coupling is represented as $\Delta v = 2$ coupling in Figure 13. In a normal mode basis this coupling could be due to a term $Q_1^3Q_2$, where the first normal mode would have NH stretch character and the second could be any one of the normal modes. We choose this term because both cubic and linear terms lead to $\Delta v = 1$ transitions in a harmonic basis. Because the NH stretch is large amplitude, it makes sense that this is the contribution raised to the power of three. In semirigid molecules this coupling is small. Because this coupling occurs through off-resonant doorway states, it is often termed an indirect coupling. 40-42

Our model takes into consideration the finding of Blodgett et al.³ that the forces \mathbf{f} along other internal coordinates increase rapidly and in a nonlinear fashion as the NH stretch is extended (see Figure 2 of that work). Rather than treat this NH stretch dependence as a Taylor series expansion, our representation of the potential of eq 1 contains the force term $\mathbf{f}^T\mathbf{S}$. Here the complicated NH stretch and bend dependencies of the force \mathbf{f} are treated on a grid of points. The corresponding matrix elements can then be evaluated with a primitive DVR basis (see eq 7). The averaged coupling that results takes the form $[\mathbf{f}]_{mn}\mathbf{S}$ in eq 6. In the context of the simplified model, it is the $[\mathbf{f}]_{14}$ term that couples the ground and first excited NH stretch state and the linear normal mode dependencies that

allow the normal modes states differing by one quantum of excitation to mix. These couplings are particularly strong in MA, and this, in conjunction with the $\Delta \nu = 1$ coupling, leads to extensive mixing of the NH stretch state. Notably, if we set $[\mathbf{f}]_{mn} = \mathbf{0}$ for $m \neq n$, we predict an NH fundamental dominated by a single transition.

The above qualitative discussion can be made more quantitative by considering the corresponding lower left 6×6 Hamiltonian matrix describing theses states. It is

$$\mathbf{H} = \begin{pmatrix} 2748 \\ 1 & 3239 \\ 8 & 0 & 2759 \\ 23 & 0 & 0 & 2279 \\ 154 & -100 & -231 & 0 & 4374 \\ 124 & 0 & -71 & -327 & -3 & 3871 \end{pmatrix}$$
(14)

The first state at 2748 cm⁻¹ is the zero-order NH stretch $\nu = 1$ state. The second and fourth states are the first overtones of the lower frequency normal modes, and the third state is the combination state with one quantum in each mode. One observes that the NH stretch is not appreciably coupled directly to the overtones and combination bands, one of which is nearby in energy. The last two states correspond to excitation of the NH stretch plus one quantum of excitation in each of the normal modes. These latter states are strongly coupled (154 and 124 cm⁻¹, respectively) to the NH fundamental via the $\Delta v = 1$ coupling of Figure 13. This coupling is proportional to $[f]_{44}$ in eq 7. The larger magnitude of the $[f]_{44}$ elements compared to $[f]_{11}$ elements is a result of the increase in forces upon excitation of the NH fundamental. Critical to the observed mixing, these states are also coupled to the overtones and combinations states via the $\Delta v = 2$ coupling

Given the role of strong indirect couplings, it is not surprising that the second-order perturbation theory treatment of AA did not produce sufficient resonant mixing of the NH stretch state with nearby states. If the above example were treated as a normal mode expansion about the equilibrium geometry, the lowest order term that leads to a force for an excited NH stretch is a term bilinear in the NH stretch and linear in another normal coordinate. The lowest order term that would lead to a coupling analogous to the $[f]_{14}$ term would be a quartic term that is cubic in the NH stretch and linear in another normal coordinate. To correctly treat near degenerate coupling between states that are indirectly coupled by cubic and quartic terms, one needs to go to third order.

The above discussion highlights the couplings that lead to the calculated spectra shown in Figure 8. We have focused this discussion on the coupling between the n=1 and n=4 {x, y} DOF basis functions. Notably, these functions do not display large-amplitude motion along the low-energy dislocation pathway shown in Figure 4. In other words, the above discussion, based on the n=1 and n=4 functions of Figure 7, cannot possibly explain the dislocation of the H atom. This motion is only evident for the higher energy states of that figure such as the n=5-6 states. These states are nearly degenerate and strongly coupled to the high-energy combination states, like those shown in Figure 13. The relevant couplings terms $[f]_{45}$ and $[f]_{46}$ (see Table S1) are 100-300 cm⁻¹ in size. As a result, the full dynamics that follows ultrafast NH excitation will involve probability passing through the n>1

4 states as the molecule relaxes back to the manifold of states built off n = 1. The extent of this flow is evident in the time-dependent results of Figure 12.

Before concluding, some comments regarding the dipole moment are in order. One might think that the interesting orientational effects observed in the dipole in Figure 5 would be an important factor to consider in the fractionation of the NH stretch fundamental. However, upon solving for the $\{x, y\}$ DOF, we find that the intensity differences between a linear dipole and the more complex behavior, observed in Figure 5, is small. This finding is not surprising given the form of the wave functions in Figure 7. Moreover, in the linear dipole approximation, a rotation of the dipole moment components does not affect the transition intensities. These results are consistent with the earlier work of Blodgett et al., 3 who reported intensities for an NH stretch—bend surface at various levels of theory of the dipole.

6. CONCLUSIONS

Methyl anthranilate and its parent molecule anthranilic acid are representative of an important class of molecules in which strong H-bonds, not present in the ground electronic state, lead, when electronically excited, to large anharmonic couplings associated with motion along a reactive potential energy surface involving H atom transfer between donor and acceptor sites. Experimentally this produces an infrared spectrum in which the most intense transition in the calculated harmonic IR spectrum is not observed experimentally. We have built a reduced-dimension Hamiltonian of 11 dimensions that shows how the NH stretch oscillator strength is spread over almost 1000 cm⁻¹, starting from frequencies well below those predicted by calculations for the S₁ NH stretch fundamental. Corresponding time-dependent calculations show that if the H-bonded NH stretch fundamental were excited with an ultrafast laser, relaxation of this state would be near complete within 40 fs.

The results of our calculations uncover a unique indirect coupling mechanism for the anharmonic mixing associated with this NH stretch fundamental. The NH stretch fundamental undergoes linear coupling with 1 + 1 combination bands involving the NH stretch and low-frequency modes, which themselves are coupled back to the overtones and combination bands of low-frequency modes that are in energetic proximity to the bright NH stretch fundamental. The magnitudes of these coupling terms are as large as 300 cm⁻¹ and lead to fractionation of the NH stretch oscillator strength over many transitions even in this reduced-dimension model. While it is possible that future experimental work can identify this spread-out, congested absorption, it is not surprising that the experimental work presently in hand does

Figure 12 shows a pictorial representation of these coupling terms and compares them with the direct coupling terms associated with 2:1 Fermi resonance or induced Franck—Condon-like intensity in combination bands built off the high-frequency fundamental. We suspect that this indirect coupling mechanism is at play much more generally than has been recognized to date. Furthermore, the discovery of this mechanism arose out of a chemically interesting circumstance in which a vibrationally adiabatic treatment of the NH stretch, involved in a strong H-bond, was found to lengthen substantially upon excitation of the NH stretch fundamental leading to near equal sharing between donor and acceptor.³ In

the more accurate treatment provided here, the short-time probability snapshots (20–40 fs) shown in Figure 7 clearly indicate probability flow along the reaction coordinate of H atom transfer. However, this flow is shown to quickly quench as the NH stretch excitation relaxes to the dense manifold of states in which this mode is de-excited.

Finally, the model developed here predicts that the ND stretch in the NHD isotopologue of MA has its ND stretch fundamental split among only one or two additional bands and should be readily detected. This is a prediction worth pursuing experimentally.

ASSOCIATED CONTENT

Supporting Information

The Supporting Information is available free of charge at https://pubs.acs.org/doi/10.1021/acs.jpca.1c04264.

A description of the internal coordinates used in the anharmonic model, the **F** and **G** matrices of the 11 degree of freedom model Hamiltonian, select $[\mathbf{F}]_{n,n}$ and $[\mathbf{f}]_{n,m}$ values from eq 6, a comparison of time-dependent results with different basis sets, and details regarding the calculation of the starting vectors for the Lanczos algorithm (PDF)

AUTHOR INFORMATION

Corresponding Authors

Edwin L. Sibert III — Department of Chemistry and Theoretical Chemistry Institute, University of Wisconsin—Madison, Madison, Wisconsin 53706, United States; orcid.org/0000-0003-2752-1044; Email: elsibert@wisc.edu

Timothy S. Zwier — Combustion Research Facility, Sandia National Laboratories, Livermore, California 94551, United States; orcid.org/0000-0002-4468-5748; Email: tszwier@sandia.gov

Author

Karl N. Blodgett — Department of Chemistry, Purdue University, West Lafayette, Indiana 47907-2084, United States; Occid.org/0000-0002-6827-0328

Complete contact information is available at: https://pubs.acs.org/10.1021/acs.jpca.1c04264

Notes

The authors declare no competing financial interest.

ACKNOWLEDGMENTS

E.L.S. gratefully acknowledges support from NSF via Grant CHE-1900095 and useful conversations with Zachery Dyott. T.S.Z. acknowledges support from the U.S. DOE, Office of Science, Office of Basic Energy Sciences, during manuscript preparation at Sandia. Sandia National Laboratories is a multimission laboratory managed and operated by National Technology and Engineering Solutions of Sandia, LLC., a wholly owned subsidiary of Honeywell International, Inc., for the U.S. DOE National Nuclear Security Administration under Contract DE-NA0003525.

REFERENCES

(1) Southern, C.; Levy, D.; Florio, G.; Longarte, A.; Zwier, T. Electronic and infrared spectroscopy of anthranilic acid in a supersonic jet. *J. Phys. Chem. A* **2003**, *107*, 4032–4040.

- (2) Stearns, J.; Das, A.; Zwier, T. Hydrogen atom. dislocation in the excited state of anthranilic acid: probing the carbonyl stretch fundamental and the effects of water complexation. *Phys. Chem. Chem. Phys.* **2004**, *6*, 2605–2610.
- (3) Blodgett, K. N.; Fischer, J. L.; Zwier, T. S.; Sibert, E. L. The missing NH stretch fundamental in S1 methyl anthranilate: IR-UV double resonance experiments and local mode theory. *Phys. Chem. Chem. Phys.* **2020**, *22*, 14077–14087.
- (4) Blodgett, K. N.; Sun, D.; Fischer, J. L.; Sibert, E. L.; Zwier, T. S. Vibronic spectroscopy of methyl anthranilate and its water complex: hydrogen atom dislocation in the excited state. *Phys. Chem. Chem. Phys.* **2019**, *21*, 21355–21369.
- (5) Sobolewski, A.; Domcke, W. Intramolecular hydrogen bonding in the S-1(π π *) excited state of anthranilic acid and salicylic acid: TDDFT calculation of excited-state geometries and infrared spectra. *J. Phys. Chem. A* **2004**, *108*, 10917–10922.
- (6) Egidi, F.; Williams-Young, D. B.; Baiardi, A.; Bloino, J.; Scalmani, G.; Frisch, M. J.; Li, X.; Barone, V. Effective Inclusion of Mechanical and Electrical Anharmonicity in Excited Electronic States: VPT2-TDDFT Route. *J. Chem. Theory Comput.* **2017**, *13*, 2789–2803.
- (7) Sibert, E. L.; Reinhardt, W. P.; Hynes, J. T. Intramolecular vibrational-relaxation and spectra of CH and CD overtones in benzene and perdeuterobenzene. *J. Chem. Phys.* **1984**, *81*, 1115–1134.
- (8) Nesbitt, D. J.; Field, R. W. Vibrational energy flow in highly excited molecules: Role of intramolecular vibrational redistribution. *J. Phys. Chem.* **1996**, 100, 12735–12756.
- (9) Florio, G. M.; Zwier, T. S.; Myshakin, E. M.; Jordan, K. D.; Sibert, E. L. Theoretical modeling of the OH stretch infrared spectrum of carboxylic acid dimers based on first-principles anharmonic couplings. *J. Chem. Phys.* **2003**, *118*, 1735–1746.
- (10) Dreyer, J. Hydrogen-bonded acetic acid dimers: Anharmonic coupling and linear infrared spectra studied with density-functional theory. *J. Chem. Phys.* **2005**, *122*, 184306.
- (11) Van Hoozen, B. L., Jr.; Petersen, P. B. Origin of the Hadzi ABC structure: An ab initio study. *J. Chem. Phys.* **2015**, *143*, 184305.
- (12) Van Hoozen, B. L., Jr.; Petersen, P. B. A combined electronic structure and molecular dynamics approach to computing the OH vibrational feature of strongly hydrogen-bonded carboxylic acids. *J. Chem. Phys.* **2017**, *147*, 224304.
- (13) Greve, C.; Preketes, N. K.; Fidder, H.; Costard, R.; Koeppe, B.; Heisler, I. A.; Mukamel, S.; Temps, F.; Nibbering, E. T. J.; Elsaesser, T. {N-H} Stretching Excitations in Adenosine-Thymidine Base Pairs in Solution: Pair Geometries, Infrared Line Shapes, and Ultrafast Vibrational Dynamics. *J. Phys. Chem. A* **2013**, *117*, 594–606.
- (14) Costard, R.; Greve, C.; Fidder, H.; Nibbering, E. T. J. J. Phys. Chem. B **2015**, 119, 2711–2725.
- (15) Sibert, E. L. Modeling vibrational anharmonicity in infrared spectra of high frequency vibrations of polyatomic molecules. *J. Chem. Phys.* **2019**, *150*, 090901.
- (16) Lin, C.-K.; Huang, Q.-R.; Kuo, J.-L. Anharmonic coupling behind vibrational spectra of solvated ammonium: lighting up overtone states by Fermi resonance through tuning solvation environments. *Phys. Chem. Chem. Phys.* **2020**, *22*, 24059–24069.
- (17) Giese, K.; Petkovic, M.; Naundorf, H.; Kuehn, O. Multidimensional quantum dynamics and infrared spectroscopy of hydrogen bonds. *Phys. Rep.* **2006**, 430, 211–276.
- (18) Myshakin, E. M.; Jordan, K. D.; Sibert, E. L.; Johnson, M. A. Large anharmonic effects in the infrared spectra of the symmetrical CH₃NO₂·H₂O and CH₃CO₂·H₂O complexes. *J. Chem. Phys.* **2003**, 119, 10138–10145.
- (19) Craig, S. M.; Menges, F. S.; Duong, C. H.; Denton, J. K.; Madison, L. R.; McCoy, A. B.; Johnson, M. A. Hidden role of intermolecular proton transfer in the anomalously diffuse vibrational spectrum of a trapped hydronium ion. *Proc. Natl. Acad. Sci. U. S. A.* **2017**, *114*, E4706–E4713.
- (20) Henderson, B. V.; Jordan, K. D. One-Dimensional Adiabatic Model Approach for Calculating Progressions in Vibrational Spectra of Ion-Water Complexes. *J. Phys. Chem. A* **2019**, *123*, 7042–7050.

- (21) Zabuga, A. V.; Kamrath, M. Z.; Rizzo, T. R. Franck-Condonlike Progressions in Infrared Spectra of Biological Molecules. *J. Phys. Chem. A* **2015**, *119*, 10494–10501.
- (22) Heine, N.; Kratz, E. G.; Bergmann, R.; Schofield, D. P.; Asmis, K. P.; Jordan, K. D.; McCoy, A. B. Vibrational Spectroscopy of the Water-Nitrate Complex in the O-H Stretching Region. *J. Phys. Chem.* A 2014, 118, 8188–8197.
- (23) Carrington, T.; Miller, W. Reaction surface description of intramolecular hydrogen-atom transfer in malonaldehyde. *J. Chem. Phys.* **1986**, *84*, 4364–4370.
- (24) Barnes, G. L.; Squires, S. M.; Sibert, E. L. Symmetric double proton tunneling in formic acid dimer: A diabatic basis approach. *J. Phys. Chem. B* **2008**, *112*, 595–603.
- (25) Frisch, M. J.; Trucks, G. W.; Schlegel, H. B.; Scuseria, G. E.; Robb, M. A.; Cheeseman, J. R.; Scalmani, G.; Barone, V.; Petersson, G. A.; Nakatsuji, H.; et al. *Gaussian 16*, Rev. C.01; Gaussian Inc.: Wallingford, CT, 2016.
- (26) Grimme, S.; Ehrlich, S.; Goerigk, L. Effect of the Damping Function in Dispersion Corrected Density Functional Theory. J. Comput. Chem. 2011, 32, 1456–1465.
- (27) Grimme, S.; Antony, J.; Ehrlich, S.; Krieg, H. A consistent and accurate ab initio parametrization of density functional dispersion correction (DFT-D) for the 94 elements H-Pu. *J. Chem. Phys.* **2010**, 132, 154104.
- (28) Zwier, T. S. Laser spectroscopy of jet-cooled biomolecules and their water-containing clusters: Water bridges and molecular conformation. *J. Phys. Chem. A* **2001**, *105*, 8827–8839.
- (29) Marechal, Y.; Witkowski, A. Infrared Spectra of H-Bonded Systems. J. Chem. Phys. 1968, 48, 3697–3705.
- (30) Dreyer, J. Unraveling the structure of hydrogen bond stretching mode infrared absorption bands: An anharmonic density functional theory study on 7-azaindole dimers. J. Chem. Phys. 2007, 127, 054309.
- (31) Borgis, D.; Hynes, J. T. Dynamic theory of proton tunneling transfer rates in solution general formulation. *Chem. Phys.* **1993**, *170*, 315–346.
- (32) Colbert, D. T.; Miller, W. H. A novel discrete variable representation for quantum mechanical reactive scattering via the Smatrix Kohn method. *J. Chem. Phys.* **1992**, *96*, 1982–1991.
- (33) Wilson, E. B.; Decius, J. C.; Cross, P. C. Molecular Vibrations; McGraw-Hill: New York, 1955.
- (34) Stanton, J. F. On the vibronic level structure in the NO₃ radical: II. Adiabatic calculation of the infrared spectrum. *Mol. Phys.* **2009**, *107*, 1059–1075.
- (35) Davidson, E. R. In *Methods in Computational Molecular Physics*; Diercksen, G. H. F., Wilson, S., Eds.; Reidel: Dordrecht, 1983; pp 95–115.
- (36) Cullum, J. K.; Willoughby, R. A. Lanczos Algorithms for Large Symmetric Eigenvalues Computations; Birkhäuser: Boston, 1985.
- (37) Askar, A.; Cakmak, A. S. Explicit integration method for the time-dependent Schrodinger equation for collision problems. *J. Chem. Phys.* **1978**, *68*, 2794–2798.
- (38) Heller, E. J.; Stechel, E. B.; Davis, M. J. Molecular-Spectra, {Fermi} Resonances, and Classical Motion. *J. Chem. Phys.* **1980**, 73, 4720–4735.
- (39) Heller, E. J. The semiclassical way to molecular spectroscopy. *Acc. Chem. Res.* **1981**, *14*, 368–375.
- (40) Hutchinson, J. S.; Sibert, E. L.; Hynes, J. T. Quantum dynamics of energy transfer between bonds in coupled Morse oscillator systems. *J. Chem. Phys.* **1984**, *81*, 1314–1326.
- (41) Cupp, S.; Lee, C.; McWhorter, D.; Pate, B. Doorway state enhanced intramolecular vibrational energy redistribution in the asymmetric = CH_2 hydride stretch of methyl vinyl ether. *J. Chem. Phys.* **1998**, *109*, 4302–4315.
- (42) Yamada, Y.; Ebata, T.; Kayano, M.; Mikami, N. Picosecond IR-UV pump-probe spectroscopic study of the dynamics of the vibrational relaxation of jet-cooled phenol. I. Intramolecular vibrational energy redistribution of the OH and CH stretching vibrations of bare phenol. J. Chem. Phys. 2004, 120, 7400–7409.